



HAL
open science

Two-step thermochemical cycles using fibrous ceria pellets for H₂ production and CO₂ reduction in packed-bed solar reactors

Stéphane Abanades, Anita Haeussler

► **To cite this version:**

Stéphane Abanades, Anita Haeussler. Two-step thermochemical cycles using fibrous ceria pellets for H₂ production and CO₂ reduction in packed-bed solar reactors. *Sustainable Materials and Technologies*, 2021, 29, pp.e00328. 10.1016/j.susmat.2021.e00328 . hal-03365928

HAL Id: hal-03365928

<https://hal.science/hal-03365928>

Submitted on 5 Oct 2021

HAL is a multi-disciplinary open access archive for the deposit and dissemination of scientific research documents, whether they are published or not. The documents may come from teaching and research institutions in France or abroad, or from public or private research centers.

L'archive ouverte pluridisciplinaire **HAL**, est destinée au dépôt et à la diffusion de documents scientifiques de niveau recherche, publiés ou non, émanant des établissements d'enseignement et de recherche français ou étrangers, des laboratoires publics ou privés.

Two-step thermochemical cycles using fibrous ceria pellets for H₂ production and CO₂ reduction in packed-bed solar reactors

Stéphane ABANADES ^{a*}, Anita HAEUSSLER ^a

^a Processes, Materials and Solar Energy Laboratory, CNRS-PROMES, 7 Rue du Four Solaire, 66120 Font-Romeu, France

* Corresponding author: Tel +33 (0)4 68 30 77 30

E-mail address: stephane.abanades@promes.cnrs.fr

Abstract:

The thermochemical redox activity and performance of commercial-grade fibrous ceria pellets were determined including fuel production rates and yields from H₂O and CO₂ dissociation. Two solar reactors integrating the ceria pellets undergoing two-step thermochemical cycling (with temperature-swing between alternating redox steps) were experimentally tested. They consisted of packed-bed tubular and cavity-type solar reactors with direct or indirect heating of the reacting materials. The obtained fuel production rates compared favorably with the performance of other previously considered microstructured ceria materials such as templated foams, sintered felts, bioinspired or ordered macroporous morphologies. H₂ production rates reached 2.3 mL.g⁻¹.min⁻¹ (with H₂/O₂ ratios approaching 2) in the indirectly-heated tubular reactor after reduction at 1400°C and oxidation upon free cooling below 950°C in steam atmosphere (57% molar content). The highest fuel production rate (~9.5 mL.g⁻¹.min⁻¹) and peak solar-to-fuel energy efficiency (~9.4%) were reached in the directly-irradiated cavity-type reactor (with a reduction step at 1400°C under reduced pressure, and an oxidation step in pure CO₂ below 950°C). The reduction extent was favored at low p_{O_2} (δ up to 0.056) and the fuel yields were thus improved notably (up to 315 μmol/g) by decreasing the total pressure below 0.1 bar during the reduction step. The fuel production rate increased when the oxidation temperature decreased (because the reaction was thermodynamically more favorable). An increase in CO₂ partial pressure further promoted the oxidation kinetics (and decreased the p_{CO}/p_{CO_2} ratio, thus shifting the thermodynamic equilibrium toward CO product). The fibrous ceria structures exhibited stable morphologies with high fuel production performance similar to less scalable porous structures, thus offering the potential for versatile applications in packed-bed solar reactors.

Keywords: solar fuel, solar reactor, ceria oxygen carrier, redox cycle, thermochemical water-splitting, hydrogen, CO₂ valorization

1. Introduction

Thermochemical processes coupling H₂O dissociation with concentrated solar power (CSP) systems appear as a promising solution to produce sustainable H₂. Similarly, such processes are also able to dissociate CO₂, thus upgrading CO₂ to CO and forming syngas when combined with H₂, which can yield hydrocarbon fuels via Fischer-Tropsch synthesis. The process based on thermochemical redox cycles is basically composed of two reactions, involving a metal oxide acting as a reaction intermediate that is recycled between steps. First, a thermal reduction of the metal oxide at high temperature is performed, resulting in the production of O₂. This reaction is thermally activated by the concentrated solar heat supplied to the system. Secondly, the reduced form of the metal oxide is re-oxidized by H₂O or CO₂, leading to the production of H₂ or CO in an exothermic reaction. The only inputs in the thermochemical process are the abundant and low cost feedstock (H₂O or CO₂) and solar heat, making it a carbon-neutral process [1,2]. The most commonly investigated cycles are based on metal oxide redox pairs such as Zn²⁺/Zn [3,4], Sn⁴⁺/Sn²⁺ [5–7], Fe³⁺/Fe²⁺ [8,9], and Ce⁴⁺/Ce³⁺ [10–12]. The thermochemical H₂O or CO₂ splitting processes offer high theoretical efficiency (because the entire solar spectrum is converted) and do not require electricity utilization. Therefore, they could be an ideal long-term pathway to decarbonize worldwide energy production. Nowadays, technological locks still need to be overcome before considering any large scale application for hydrogen or syngas production using solar thermochemical processes. The major challenge is to develop reliable thermochemical processes with high and stable fuel production along with fast reaction rates, meeting industrial requirements.

In this context, this study aims to investigate the solar thermochemical conversion of H₂O and CO₂ for the production of high-value solar fuels, using non-stoichiometric metal oxides as chemical intermediates. Such oxygen carrier materials encompass fluorite-based (e.g., ceria-CeO₂) and perovskite (ABO₃) structures, in which the oxygen vacancies created during the reduction step absorb the oxygen from CO₂ or H₂O, thereby producing CO or H₂ [13–17]. The oxygen non-stoichiometry (δ in CeO_{2- δ} or ABO_{3- δ}) determines the amount of fuel that can be produced by the two-step redox process:



The main current research fields and priorities are related to: (i) the development and evaluation of the materials potential for thermochemical cycles via a study of their redox activity, in order to select the most performant and stable redox materials to be integrated in a solar reactor; (ii) the synthesis and shaping of the reactive materials as porous structures; (iii) the design and construction of scalable and flexible solar reactor prototypes based on different heating concepts and operating modes. Such reactor concepts basically consist of monolithic or particle-based configurations with temperature-swing redox cycling. The main evaluated ceria morphologies for this

application were three-dimensionally ordered macroporous (3DOM) structures [18,19], bioinspired materials [20,21], porous monoliths [22–25], fibers [26,27], and reticulated porous ceramics (RPC) [28,29]. Alternatively, the membrane configuration was also proposed involving mixed ionic-electronic conducting membranes for isothermal and continuous operation [30–32]. Among the suitable redox materials, ceria has been identified as a benchmark oxygen carrier candidate given its high oxygen storage and exchange capacity, structural stability over a large range of oxygen non-stoichiometry, and fast kinetics during the redox process [11,33,34]. The availability of commercial-grade reactive ceria materials with suitable morphologies and microstructures is advantageous for short to mid-term large-scale application of solar thermochemical cycles. Moreover, the experimental performance assessment of redox materials under representative conditions in solar reactors is scarce to date, but of major importance to provide insights into the performance of real on-sun reactor systems.

In this work, the objective was to experimentally demonstrate the H₂O and CO₂ splitting process during on-sun operation of two different solar reactors (directly and indirectly-irradiated) and to compare their performance, using commercial-grade fibrous ceria pellets. The material porous microstructure and morphology was particularly relevant for the gas-solid reactions, and the performance stability was shown to be remarkable at the considered processing conditions. The global cylindrical shape of the pellets was also suitable for their utilization as a packed-bed, with favorable scalability in view of future industrial application. The suitability of such materials processed within both directly and indirectly-heated solar reactors was further assessed to confirm their compatibility with various reactor designs and applications. The evaluation of the thermochemical performance of the ceria redox materials, integrated within the developed solar reactors, was realized in this work to determine the fuel production capacity using real concentrated solar radiation.

2. Solar reactors for thermochemical H₂O- and CO₂-splitting cycles

Two solar reactors based on the packed-bed concept with different designs were used to perform thermochemical cycles. The performances of ceria materials integrated in the solar reactors were experimentally assessed to determine the effect of the most relevant operating parameters including the temperature, reduction pressure, type and concentration of oxidant gas (H₂O or CO₂) impacting the solar fuel production. Optimized thermochemical reactor performance need to be identified for suitable operating parameters, which is essential to prepare process scale-up. Specifically, the amounts and rates of fuel production must be assessed in prototype-scale reactors under representative operating conditions. Such experimental investigation carried out with real solar reactors operated with relevant ceria pellet porous structures has not been performed before.

2.1. Indirectly-heated tubular solar reactor

The solar tubular thermochemical reactor was devoted to the investigation of high-temperature solid-gas reactions in controlled atmospheres [21,35,36]. It was placed at the focus of a medium size horizontal-axis solar furnace, consisting of a sun-tracking heliostat reflecting incident solar irradiation towards a 2 m-diameter parabolic dish concentrator. Concentrated solar energy was used as the high-temperature process heat to drive the redox reactions. The solar reactor was composed of a cavity receiver made of graphite with a 20 mm-diameter front aperture (at the focal point of the concentrator) to absorb the concentrated solar power. The reactor cavity was insulated and closed at the front by a transparent glass window. The maximum power absorbed by the cavity through the aperture was about 1.5 kW (for a Direct Normal Irradiance DNI of $1 \text{ kW}\cdot\text{m}^{-2}$). The ceria packed-bed sample was settled inside a vertical alumina tube (20 mm internal diameter) crossing the absorbing cavity. This cavity-type configuration provides homogeneous temperature distribution along the tubular reacting zone (40 mm height) where the sample is placed.

The temperature was measured thanks to a B-type thermocouple directly inside the reacting sample and by a solar-blind pyrometer pointing to the tube external wall. The inlet gas flow rate (Ar carrier gas, 99.999% purity, O₂ content below 2 ppm) and liquid H₂O flowrate were regulated using electronic mass flow controllers (water was injected into the tube via a stainless steel capillary and was vaporized, so that entrained steam could react with the sample). The gases flowed from the top to the bottom of the tube and the outlet products (O₂ and H₂) were transported by the carrier gas to gas analyzers. The outlet gas first flowed through a bubbler to eliminate excess steam and a gas drying unit (desiccant column). The O₂ concentration in the outlet gas was measured continually with a zirconium oxide sensor (SETNAG™ JC48V, range: 10–10000 ppm, precision: 0.2%), and the H₂ concentration was measured by thermal conductivity detection (Emerson NGA2000; range: 0–10% H₂, precision: <1% of full-scale). The gas production yields were then quantified by time integration of the gas production rates.

After purging the reactor from residual air by vacuum pumping and Ar refilling, the reactor was heated in Ar to carry out the endothermic ceria reduction (up to ~1400°C) while measuring the evolution of O₂ concentration. Once the reduction was completed (i.e. O₂ release became low enough and equilibrium oxygen under-stoichiometry in ceria was reached), the solar power was shut down for reactor cooling to perform the oxidation step. A shutter positioned on the path of the reflected sunlight was used to control the solar energy input, thereby adjusting the temperature. With the temperature decrease after closing the shutter, the O₂ concentration dropped to almost zero. Subsequently, steam (balanced with Ar) was injected to react with the oxygen-deficient ceria and to produce H₂ during the oxidation step, which was performed without any solar energy supply (free reactor cooling). Once the oxidation was complete, as ascertained by the H₂ concentration returning to zero, the reactor was heated again to proceed for the next cycle.

2.2. Directly-heated solar reactor

The directly-irradiated solar reactor (SUNFUEL) was previously developed for two-step redox cycles using various forms of reacting materials including reticulated ceria foams, perovskite-coated foams, or porous biomimetic cork-templated ceria granules [27,29,37,38]. It was placed at the focus of a medium-size vertical axis solar furnace (same characteristics as those mentioned in the previous section). The 1.5 kW_{th} solar reactor was composed of an insulated alumina cavity (60×50 mm tube, 80 mm height) closed by an alumina front cover (with a 18 mm-diameter aperture) along with a glass window to let the concentrated sunlight entering the cavity (Figure 1). The temperature was measured at different locations by B-type thermocouples (T1, T2, and T3) and by a solar-blind pyrometer (at 4.8-5.2 μm). The reactor pressure was monitored with three pressure sensors (at gas inlets and within the cavity).

The cavity configuration was designed to investigate particulates or pellets materials in divided forms (Figure 2). In order to position the ceria pellets in a suitable way for their efficient heating by solar radiation, an alumina confiner tube was placed at the cavity center to maintain the main part of the reactive pellets as a packed-bed in the annular region around the tube. In addition, a small portion of pellets was placed inside the tube, thereby enabling uniform heating of the sample height thanks to radiative heat transfer inside the central tube cavity as well as conduction-convection across the material bed. During redox steps, the gas continuously flowed through the pellets, which favored heat and mass transfer, gas products transport and removal, thus shifting reactions to the products side until reaching reaction completion.

During the reduction step, the reactor was heated by opening the shutter positioned below the reactor until reaching the target temperature (1400°C at T1). The carrier gas (Ar, 99.999 % purity with [O₂] < 2 ppm) was injected below the glass window for gas sweeping (1 NL/min), while a smaller flow rate (0.2 NL/min) entered the cavity via a lateral inlet. Ar then flowed through the reactive pellets and exited via the outlet at the cavity bottom with the released oxygen. The O₂ concentration was measured by a trace oxygen electrochemical analyzer (Systech, range: 0.1 ppm to 1%, precision ±2% of reading). A vacuum pump at the reactor outlet was possibly used when operating the reduction step under low pressure (~0.1 bar) in flowing Ar, in order to investigate the influence of total pressure on the reduction extent (and the associated fuel production yield during oxidation). Once the reduction rate became low enough (O₂ concentration below 500 ppm), the shutter was closed to cool down the reactor. For the oxidation step (performed off-sun at atmospheric pressure), the oxidant gas (either CO₂ or H₂O) at the desired mole fraction was injected via the lateral inlet of the cavity upon free cooling (from typically 1050°C). Water flowed through a capillary before being vaporized when approaching the cavity entrance and then, steam was transported by the carrier gas to flow through the reacting ceria. The gas and liquid flow rates were regulated thanks to mass flow controllers (MFC, Brooks Instruments model SLA5850S). Right after oxidant injection, a peak rate of fuel production was measured promptly. Regarding CO₂-splitting cycles, both CO₂ and CO outlet concentrations were analyzed online by NDIR sensors (MGA3000, full scale: 0-30% for CO, 0-100% for CO₂, precision

$\pm 1\%$ of full scale). Regarding H₂O-splitting cycles, H₂ was analyzed continuously by thermal conductivity detection (catharometer for Ar/H₂ binary mixture, scale: 0-10%, precision: 1% of full scale) after flowing through a gas dryer (to eliminate excess water). The gas production amounts (yields, mole per gram of ceria) for each cycle were then quantified from time integration of the production rates (F_i) over the cycle duration.

$$n_i = \int F_i \cdot dt \quad (3)$$

The gas production rates during each cycle step (F_i where i denotes O₂, H₂, and CO) were first determined from the outlet gas composition (mole fractions, y_i) measured by online gas analysis as a function of time.

$$F_{O_2} = F_{Ar} \cdot y_{O_2} / (1 - y_{O_2}) \quad (4)$$

$$F_{H_2} = F_{Ar} \cdot y_{H_2} / (1 - y_{H_2}) \quad (5)$$

$$F_{CO} = (F_{Ar} + F_{CO_2}) \cdot y_{CO} \quad (6)$$

Where F_{Ar} and F_{CO_2} are the inlet flow rates of Ar and CO₂ (mol/s).

The gas production rates and yields for each cycle (provided in Table 1) were finally expressed relative to the unit mass of loaded oxide (in mL/min/g for the production rates and $\mu\text{mol/g}$ for the production yields) for data comparison.

The oxygen non-stoichiometry in ceria after the reduction step was calculated by:

$$\delta = 2 M_{CeO_2} n_{O_2} \quad (7)$$

where M_{CeO_2} is the molecular weight of ceria (g/mol) and n_{O_2} is the amount of O₂ produced (mol/g).

The re-oxidation extent was obtained from the amount of fuel produced, n_{fuel} (mol/g):

$$X_{ox} = n_{fuel} / 2n_{O_2} \quad (8)$$

The solar-to-fuel efficiency ($\eta_{solar-to-fuel}$) was calculated as follows:

$$\eta_{solar-to-fuel} = r_{fuel} \text{HHV}_{fuel} / P_{solar} \quad (9)$$

where r_{fuel} is the fuel production rate (mol/s), HHV_{fuel} is the higher heating value of the fuel (J/mol), and P_{solar} is the solar power input (W).

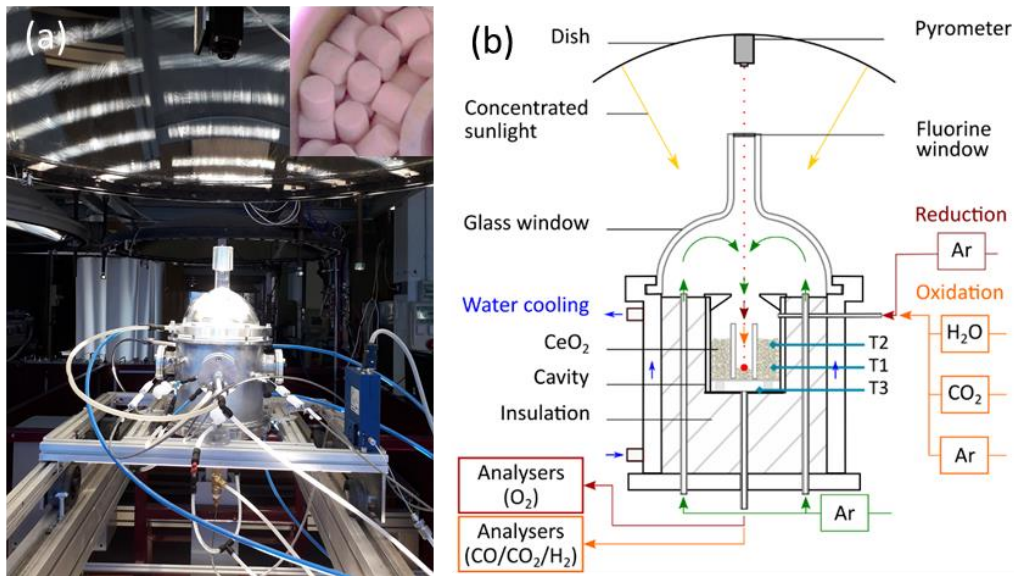


Figure 1: (a) Photograph of the SUNFUEL solar reactor (image insert on the right shows ceria pellets inside the alumina cavity), and (b) schematic illustration of the solar reactor, red arrows represent the gas flow during the reduction step, orange arrows the gas flow during the oxidation step, green arrows the Ar flow injected during both steps to protect the glass window and sweep the cavity, and blue arrows the water-cooling.

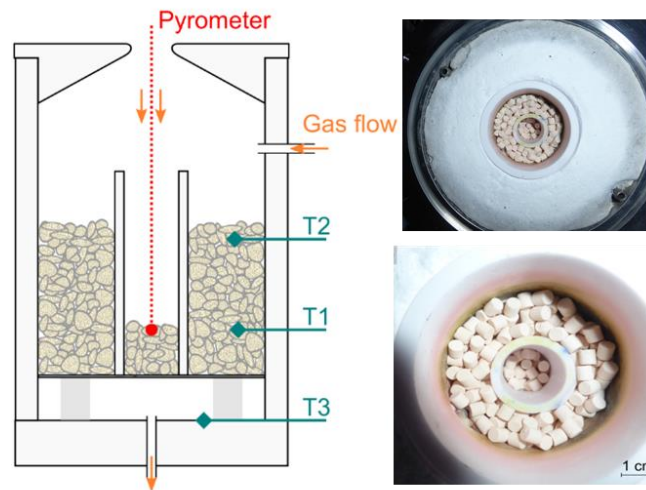


Figure 2: Scheme of the cavity configuration and images of the investigated ceria pellet materials inside the alumina cavity.

3. Ceria pellets characteristics and expected benefits for the solar process

The fibrous ceria pellets (CeP, >99.8% purity) were supplied from Zircar Zirconia Inc. USA (density of individual pellets: 1842 kg/m³, porosity ~74%, poured density: 1089 kg/m³), and their shape was cylindrical (4 mm in height and 4 mm in diameter). Pictures of the reactive materials are presented in Figures 1-2. Prior to solar experiments, the pellets were calcined at 1400°C (typical

maximum temperature of the thermochemical cycles) for 4 h in order to stabilize their morphology before cycling, and eliminate possible volatiles and trace of moisture.

The morphology of the materials before and after cycling was studied by scanning electron microscopy (SEM). Samples were mounted on stubs with carbon tape, and then imaged on a Philips XL30 FEG microscope using an acceleration voltage of 3-10 kV. The specific surface area (S_{BET}) was determined by the BET method from N_2 adsorption at -196°C (Micromeritics ASAP 2020), after degassing at 4×10^{-3} mbar and 300°C for 12 h.

The ceria pellets were fabricated by forming ceria fibers and sintering into a cylindrical pellet shape. The integration of such porous materials in solar reactors for solar fuel production was never considered before. It is widely recognized that the use of bulk powders as packed-beds in solar reactors is not suitable due to agglomeration/densification. This is because the particle bed usually gets dense under the heating effect, which hinders the gas flow inside the bed and strongly limits the reaction kinetics. In addition, it induces a pressure drop and also restrains the solar radiation absorption to the surface only (high opacity), creating large thermal gradients across the bed and non-uniform reaction extent. Overheating of the surface may cause bed densification, which represents a known limitation for the process stability and induces a loss in fuel production capacity during cycling in the case of particles. Conversely, the use of densified fibrous pellets warrants a good access of the gaseous species to the bulk reacting ceria, while it further allows loading a sufficient amount of ceria to enhance the fuel production capacity. Such mm-sized pellet particles have suitable characteristics for use in packed-bed solar reactors.

Another approach consists in integrating the ceria material in the form of RPC foams inside the reactor cavity. Such reactive porous structures combine the advantages of low optical thickness (i.e., low opacity) for efficient volumetric radiative absorption and uniform heating, and low pressure drop. This is commonly the case for high porosity and large pore size foams (~90% porosity, 10-20 ppi-pore per inch). However, the oxidation step of ceria with H_2O or CO_2 requires a large available contact surface to promote kinetics, which further necessitates a porous microstructure within the foam struts to increase both the surface area and the access of the oxidant gas to the ceria bulk for rapid reaction rates. Such interconnected porous network often weakens the structure thermos-mechanical resistance and lowers the density, thus the ceria mass loading. Combining all the desired properties is thus clearly not possible, because low optical thickness (for volumetric radiative absorption), high surface area (for rapid reaction rates), and low porosity (for high material mass loading in the reactor) have antagonist effects and a trade-off must be reached.

On the other hand, the use of fibrous pellets offering high porosity for rapid reaction rates and facilitated integration can be a relevant option to operate packed-bed solar reactors, provided that uniform heating can be effectively reached [39]. In this application, the actual density of the pellets combined with their regular shape results in a bulk density inside the reactor chamber that allows

reaching the desired theoretical ideal mass of ceria in the reactor (i.e. close to the mass of ceria bulk powder).

This specific shaping is advantageous compared to fluidized bed or particle-entrained flow reactors, because it does not rely on the use of a high gas flow rate for operating the reactor. In this case, such a constraint is eliminated since the reactive pellets remain fixed inside the reactor, while non-stoichiometric ceria undergoes solid-state redox reactions. Eliminating particle transport between reaction steps is beneficial because the need for continuous particle feeding and collection is bypassed [40]. Avoiding solid flow is advantageous for scaled-up process, while the gas flow rate can be kept at minimum value. In this case, the inert gas flow only serves as a purge sweeping gas to transport the evolved gas species (O_2 and H_2/CO) to the reactor outlet, and can be adjusted to tune the oxygen partial pressure during reduction (dilution) and the oxidant gas concentration (steam or CO_2) during oxidation.

4. Results and discussion

4.1. Materials cycling in fixed-bed tubular solar reactor

The reducibility and H_2O -splitting ability of CeO_2 pellets settled as a loose packed-bed (~10 g resulting in a bed height of ~30 mm) were assessed via successive thermochemical cycles in the tubular solar reactor (indirectly-heated) under real solar irradiation conditions. Both the O_2 and H_2 rate evolutions, as well as the measured temperatures (inside the reactant by a B-type thermocouple T_{sample} and at the tube external wall by a pyrometer T_{pyro}), are depicted in Figure 3. The temperature of the reduction step in the sample bed was typically maintained at ~1400°C, and was controlled by adjusting the shutter opening in response to possible dynamic variations of the DNI owing to the diurnal transient evolution, or to weather instabilities (passing clouds). The first cycle was performed separately to assess the material's reactivity and lasted less than one hour (Figure 3a), with a resulting H_2 production yield of ~126 $\mu\text{mol/g}$ and an H_2/O_2 ratio of ~1.96, denoting the quasi-complete sample re-oxidation upon steam exposure after reduction in Ar (at 1400°C and P_{atm}). The O_2 production rate was strongly dependent on the heating rate and O_2 started to evolve at ~890°C, but it was highly sensitive to temperature changes and heating rates. Indeed, the O_2 release decreased when the heating rate was lowered and then increased again when boosting the heating, thus highlighting that the reduction rate is controlled mainly by the heat transfer rate. As a result, the O_2 production featured a broadened pattern and was completed once reaching the steady state temperature dwelled at 1400°C for 5 min. The solar power input was then stopped and the temperature decreased during free reactor cooling. During off-sun oxidation, the H_2 production rate showed a sharp peak (starting at ~1010°C) a few seconds after H_2O was injected, and subsequently decreased steadily until reaching complete sample re-oxidation (yielding a total H_2 peak duration of ~9 min).

Hence, the re-oxidation reaction started promptly as soon as steam was injected in the reactor upon cooling. The continuous temperature decrease favored the oxidation reaction because this exothermal step is thermodynamically enhanced at low temperature. In contrast, the O₂-releasing reaction is the endothermal step and requires high temperatures, which explains why O₂ evolved continually during sample heating (and the reduction reaction did not start before reaching a minimum temperature while the kinetic rate was slow). The difference in O₂ and H₂ rate evolution profiles points out the main governing mechanisms that control the redox process with ceria oxygen carrier. The reduction reaction is controlled by oxygen ions solid-state diffusion in the ceria lattice via migration of oxygen vacancies and electrons, and this step is thermally activated (limited by heat transfer). It is characterized by a continuous oxygen disincorporation from the oxide lattice as the temperature is increased. The reduction rate (O₂ evolution profile) thus immediately varied in response to the change of the temperature. On the other hand, the oxidation reaction generating H₂ first involves a surface reaction (limited by the available solid-gas surface area), followed by internal diffusion of the oxidant gas within the porous structure of the bulk oxide. The sharp peak is thus the result of the rapid surface reaction followed by gas diffusion through the interconnected porous network, which justifies the use of highly porous materials (with open porosity) for this reaction.

In the subsequent six cycles performed in series for about 5 h during another day (Figure 3b), the release of O₂ started at about 900°C similarly to the first cycle, and a peak O₂ concentration was again achieved once reaching the nominal temperature set-point (held at a dwell for ~10 min). The H₂ production was about 60 µmol/g when the sample reduction temperature was only 1300°C (two consecutive cycles), whereas it increased to ~150 µmol/g at a reduction temperature of 1400°C (three consecutive cycles). The peak H₂ production rate increased markedly (from about 1.7x10⁻³ to 2.3x10⁻³ NL.min⁻¹.g⁻¹) when decreasing the temperature of steam injection (from 1030°C to 940°C), which demonstrates the strong sensitivity of the oxidation rate to the temperature. The low oxidation temperature thus promotes the oxidation rate, while the total H₂ production yield remains unchanged because the oxidation is complete and the fuel capacity is related to the reduction extent (δ).

The last cycle was performed at a low reduction temperature (1170°C) and a very low H₂ production was then measured, which confirms that high reduction temperatures (above 1300°C) are mandatory to conduct the ceria redox cycle. The H₂/O₂ ratio was very close to 2 regardless of the cycle number and conditions, which provides compelling evidence of the complete fibrous material oxidation due to favorable morphology.

Table 1 summarizes the cycling conditions (including reduction and oxidation temperatures, Ar and H₂O flow rates for each cycle) along with the O₂ and H₂ production yields calculated by time integration of the production rate profiles.

The performance obtained for the fibrous ceria pellets can be compared with previous results obtained in the same reactor configuration for bio-sourced materials (cork-templated ceria, CTCe) and

ceria foams [41]. For CTCe reduced at 1400°C, the oxygen yield was 74 $\mu\text{mol.g}^{-1}$ ($\delta=0.025$, corresponding to a reduction extent of ~5%) and the maximum H₂ production at 1050°C was 162 $\mu\text{mol.g}^{-1}$, which is in line with this study (cycle #4) as well as with previously reported data for pure ceria powders [42]. The reduced CTCe material totally reacted with steam and the oxidation step temperature influenced the re-oxidation rate: the lower the temperature, the higher the H₂ production rate (while the H₂ production yield is not affected significantly). This can be explained by thermodynamic limitations, i.e., the exothermic reaction is not favored by a temperature increase. However, the peak H₂ rate remained always below 1.5 $\text{mL.min}^{-1}.\text{g}^{-1}$ for CTCe, thus lower than the maximum production rates obtained with ceria pellets.

Regarding the polyurethane templated ceria foam (CeF), the mean O₂ specific yield after reduction at 1400°C was ~50 $\mu\text{mol.g}^{-1}$ whereas the H₂ yield reached a maximum of 115 $\mu\text{mol.g}^{-1}$ (corresponding to a production rate of ~0.7 $\text{mL.min}^{-1}.\text{g}^{-1}$) [41]. The oxidation kinetics was also improved when decreasing the temperature of steam injection from 1150 to 950°C, in line with thermodynamics. The superior reactivity of the fibrous ceria pellets when compared to cork-structured (CTCe) or ceria foam (CeF) is demonstrated by the significantly enhanced H₂ production rate (typically 1.6-2.3 $\text{mL.min}^{-1}.\text{g}^{-1}$ for CeP vs. 1.0–1.4 $\text{mL.min}^{-1}.\text{g}^{-1}$ for CTCe and 0.6–0.8 $\text{mL.min}^{-1}.\text{g}^{-1}$ for CeF). Note that the superior activity of the cork-derived ceria ecoceramics over the polymer replicated ceria foams was also previously observed in the case of solar-driven thermochemical splitting of CO₂ [21].

Basically, the rationale for the improved fuel production rates observed for the ceria pellets is related to the fibrous morphology combined with interconnected open porosity. This offers larger material surface being exposed to the gas stream and facilitates the transport of gaseous species, thus promoting ceria oxidation under an oxidant flow.

When comparing data obtained in the present study (H₂O-splitting by solar heating) with those previously reported in different systems (cycles carried out using conventional heating sources), it can be concluded that CeP reduced at 1400°C clearly performs better than most of the other tested materials [22,28,43–48], as summarized in Table 2. For instance, a ceria felt made of compressed ceria fibers yielded slightly higher fuel yields because it was reduced at a higher temperature of ~1650°C and oxidized at a lower temperature below 900°C [45]. However, extended material degradation was observed after exposure to high-flux radiation, and the low thermal conductivity of the ceria felt resulted in undesired temperature gradients across the felt, as also noticed for directly-irradiated ceria fiber boards [27]. Macroporous structures for volumetric solar radiation absorption and homogeneous temperature distribution were also considered. A porous ceria monolith offered an H₂ production rate of ~3.2 $\text{mL.min}^{-1}.\text{g}^{-1}$ (down to ~1.5 $\text{mL.min}^{-1}.\text{g}^{-1}$ after 100 cycles) when cycled between 1500°C and 800°C [22]. Single and dual-scale porosity foams also yielded lower fuel production rates (up to ~1.2 mL/min/g with reduction at 1450-1500°C at 10 mbar) [28,44,47]. Beyond fuel production rates, the material stability is essential to avoid undesirable losses in fuel production due to sintering issues.

Thus, the decrease of the ceria cycle temperature is required. The promising H₂ production rates obtained in this work for a reduction step performed at 1400°C provide evidence of the attractive redox activity of CeP. Hence, this material was further cycled in a novel directly-irradiated cavity-type solar reactor using a higher amount of reactive ceria, because experimental studies are of major importance to provide insights into the performance of real on-sun reactor systems.

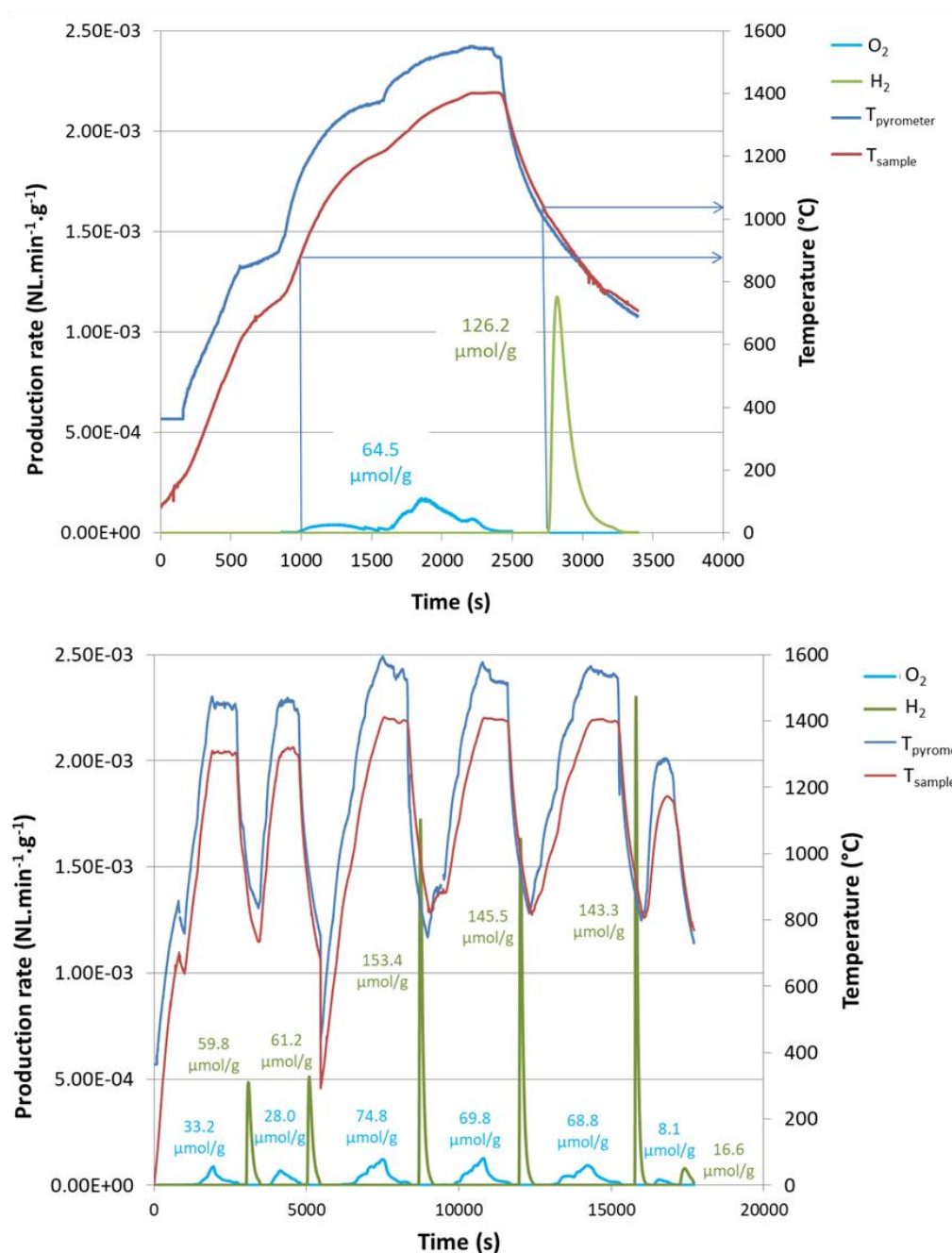


Figure 3: Time-dependent O₂ and H₂ rate profiles during solar thermochemical reduction and re-oxidation cycles for fibrous ceria pellets (CeP) in the fixed-bed tubular solar reactor: (a) first cycle (day 1), (b) six consecutive cycles (day 2).

4.2. Materials performance in directly-heated solar reactor

The thermochemical redox activity of ceria pellets in successive cycles was investigated in the directly-irradiated solar reactor. The reactor is suited for processing a higher amount of reactive material (~60 g) in comparison with the tubular reactor (~10 g). Increasing the loaded oxide mass inherently enhances the global solar-to-fuel energy conversion efficiency since the absorbed solar power is similar (1.35 kW). Obviously, the efficiency can be further enhanced by reactor up-scaling for reducing heat losses and increasing the amount of processed ceria in the solar reactor.

In order to investigate the thermochemical redox activity of the material in the solar reactor, consecutive cycles were performed with different operating conditions (Figure 4). These cycling experiments aimed to demonstrate the solar process reliability, controllability, and robustness under various processing conditions with real high-flux solar irradiation (i.e. under representative conditions of a real process). Cycling experiments were also performed to demonstrate the materials' stability. The relevant operating parameters (pressure, temperature, and inlet gas flow rates/compositions) were varied to optimize the thermochemical redox performance and to unravel the performance sensitivity to the process conditions. A total of 11 cycles was performed with CeP (7 cycles with CO₂ and 4 with H₂O), corresponding to ~18 h of continuous on-sun operation (i.e. solar reactor continually heated by concentrated sunlight, except during night shutdown, and tests performed during 4 consecutive days)

The operating conditions used for each cycle and the corresponding gas production yields are summarized in Table 1. The highest peak fuel production rate obtained in this study with CeP reached ~9.5 mL.g⁻¹.min⁻¹ (cycle #11 with reduction at ~1400°C under reduced pressure of 83 mbar, and oxidation under 100% CO₂ upon cooling starting at ~950°C), as represented in Figure 4. Note that cycles #4 and #10 also yielded high CO production rates (~7.5-7.8 mL.g⁻¹.min⁻¹) due to the low pressure during reduction, but the re-oxidation step was performed upon cooling starting at <1050°C (this higher temperature is less favorable for the oxidation step). For the cycles performed at low pressure during reduction, the O₂ production was boosted by 50% (δ up to 0.056 in cycle #4) and the CO production yield was over 300 μmol/g (162.4 μmol/g O₂ and 315.0 μmol/g CO in cycle #4). In addition, a complete re-oxidation was achieved in most of performed cycles (oxidation extent above 99%). In comparison, other studies [47–49] reached a peak CO production rate of 1.2 mL.g⁻¹.min⁻¹ using ceria foams cycled with more favorable operating conditions for the reduction step (T_{red}=1500°C under 10 mbar).

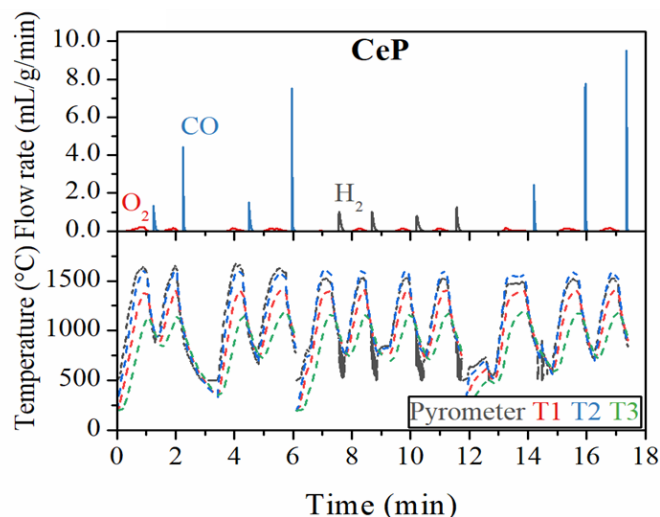


Figure 4: O₂ and fuel production rates during the performed cycles (11 cycles) along with the temperature profiles for CeP in the directly-heated solar reactor. T1, T2 and T3 are the temperatures of the sample interior, sample surface and base of the reactor.

In another study with the same reactor [27], the highest peak CO production rate reached $3.1 \text{ mL}\cdot\text{g}^{-1}\cdot\text{min}^{-1}$ for CTCe, whereas a previous study [21] using cork-templated ceria granules in a tubular packed-bed solar reactor reported a peak CO production rate of $1.9 \text{ mL}\cdot\text{g}^{-1}\cdot\text{min}^{-1}$ under similar conditions (reduction step at $\sim 1400^\circ\text{C}$ and atmospheric pressure). Clearly, an improvement of the peak fuel production rate was obtained in this work using CeP in comparison with previously reported data (Table 2), confirming the relevance of the studied materials integrated within the developed solar reactor.

For a given nominal temperature (measured at T1), the O₂ and CO amounts produced in the directly-irradiated solar reactor were higher than those obtained in the indirectly-irradiated tubular solar reactor (Table 1). This was due to a temperature gradient in the cavity that was not encountered in the packed-bed tubular reactor. This in turn means that higher temperatures were likely to occur in the upper part of the cavity (above T1), as suggested by T2 and $T_{\text{pyrometer}}$ being higher than T1 (Figure 5). Thus, the higher O₂ and CO production yields obtained for CeP in the solar reactor, in comparison with other tested materials (CTCe and CeF, as shown in Figure 5), could be explained by the more pronounced temperature gradient along the bed height ($\sim 200^\circ\text{C}$ gap between T2 and T1), due to the lower thermal conductivity of the sintered fiber particles. This is because the upper side of the material was exposed to the high-flux solar radiation inside the cavity (Figure 2), thus increasing dramatically the temperature of the material surface, while heat transfer through the bed was largely dependent on conduction in addition to convection and radiation. The control temperature in the reactor was always maintained at T1 (1400°C), in order to ensure that the whole reactive bed reached this temperature

during the reduction step. The higher temperature reached by the part of the material situated above T1 induced a larger reduction extent in this zone. The average oxygen non-stoichiometry δ reached by the whole CeP material ($\delta \sim 0.039$) was thus higher (~ 0.026 and 0.023 for CeF and CTCe, respectively) in the reference cycle presented in Figure 5.

The maximum fuel production rate was achieved with a reduction step at low pressure and an oxidation step upon cooling starting at 950°C in pure CO_2 (Figure 6). A lower pressure during reduction promoted the reduction extent (δ up to 0.056 in cycle #4 and 0.051 in cycle #11) and a lower temperature during oxidation was thermodynamically more favorable. This is consistent with previous studies performed with ceria foams, in which the effect of the operating conditions was assessed [27,38].

Accordingly, the fuel production rate also increased when the inlet CO_2 mole fraction was increased ($4.42 \text{ mL.g}^{-1}.\text{min}^{-1}$ in cycle #2 for $100\% \text{ CO}_2$ vs. $1.53 \text{ mL.g}^{-1}.\text{min}^{-1}$ in cycle #3 for $25\% \text{ CO}_2$), because the oxidation reaction was favored due to both favorable kinetics (increase of p_{CO_2}) and thermodynamics (decrease of $p_{\text{CO}}/p_{\text{CO}_2}$ ratio thus shifting the reaction toward CO formation). It was also observed that CO_2 -splitting was favored over H_2O -splitting (consistently with thermodynamics), since the H_2 production rates were lower (for the same reduction extents at 1400°C), whereas the H_2 production yields were similar ($\sim 190\text{-}200 \mu\text{mol/g}$), in agreement with previous works [29,37].

A relevant figure of merit for the solar process is the solar-to-fuel energy conversion efficiency ($\eta_{\text{solar-to-fuel}}$), defined as the ratio of the energy content of the produced fuel to the solar power input during the on-sun reduction step (the oxidation step was performed off-sun) [29,37]. Taking into account the peak CO production rate for CeP (and the higher heating value of $\text{CO} = 284 \text{ kJ.mol}^{-1}$), the maximum solar-to-fuel energy conversion efficiency $\eta_{\text{solar-to-fuel}}$ was $\sim 9.4\%$, for 1.35 kW of solar thermal power input absorbed in the reactor cavity. In contrast, $\eta_{\text{solar-to-fuel}}$ was $\sim 1.5\%$ for the reference conditions shown in Figure 5.

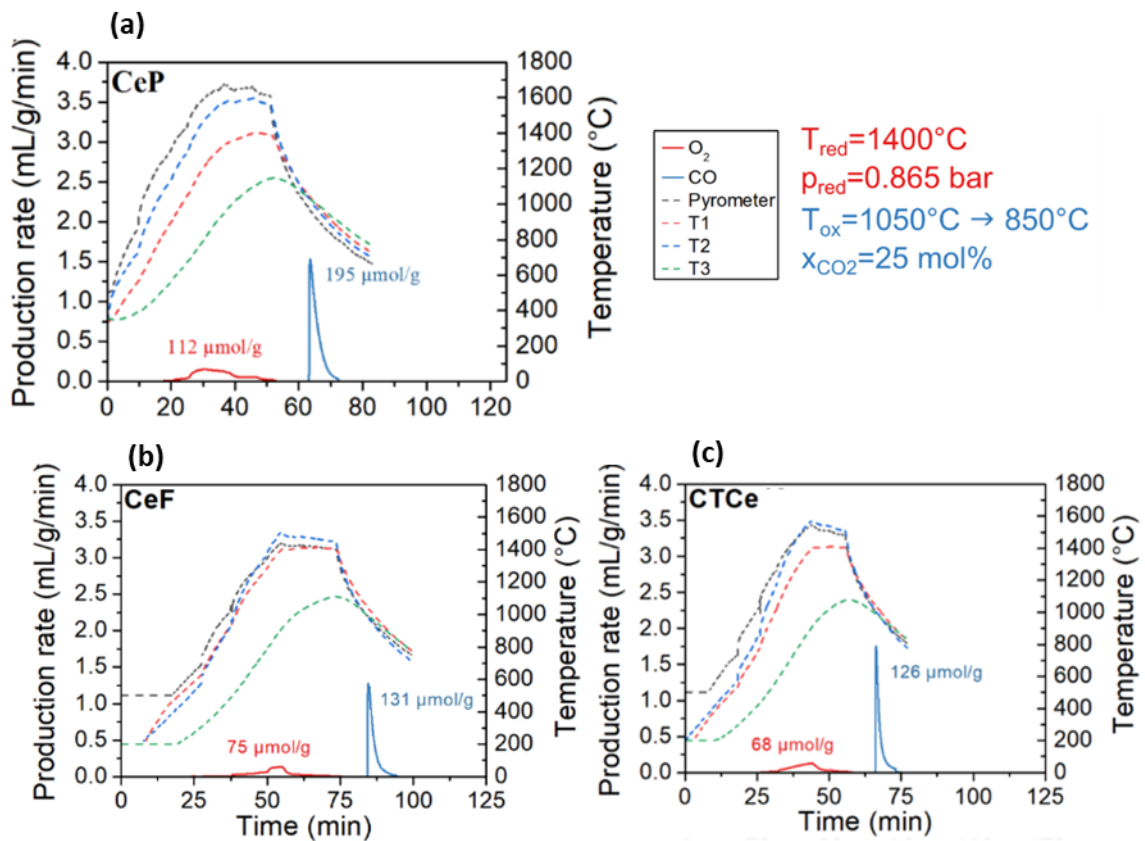


Figure 5: Thermochemical cycles at atmospheric pressure, $T_{red}=1400^{\circ}\text{C}$ and $T_{ox}=1050\text{-}850^{\circ}\text{C}$ with 25mol% CO₂ during the oxidation step for (a) CeP (cycle #3), compared with (b) CeF and (c) CTCe [27].

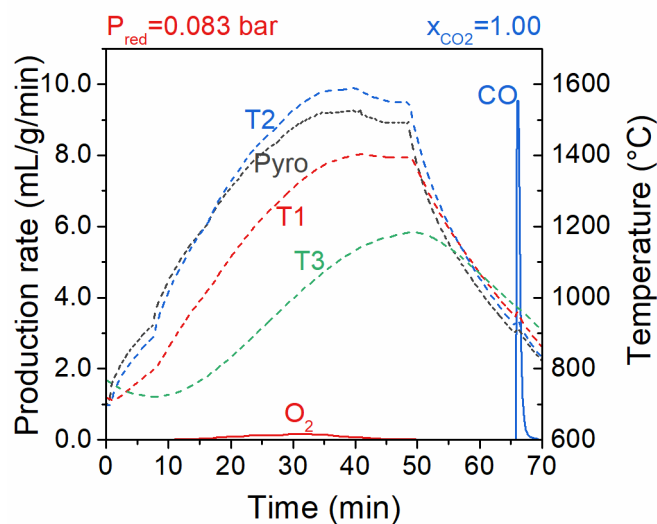


Figure 6: Thermochemical cycle for CeP (cycle #11 with reduction step performed at reduced pressure, $T_{red}=1400^{\circ}\text{C}$ and $T_{ox}=950\text{-}850^{\circ}\text{C}$ with 100mol% CO₂ during the oxidation step).

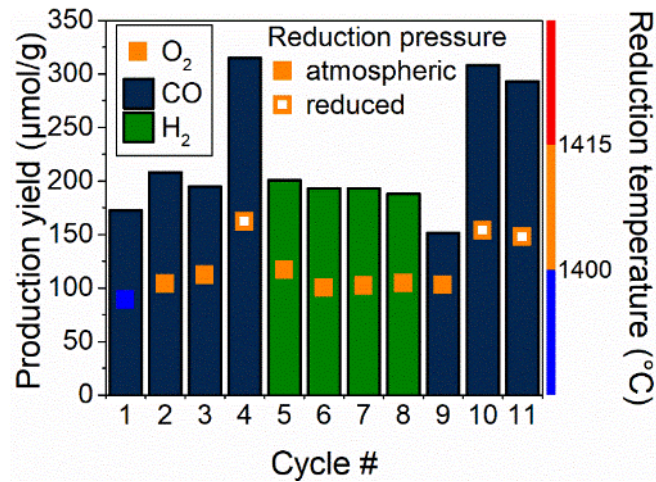


Figure 7: O₂ and fuel production yields over cycles for CeP; squares represent the O₂ production amount and bars refer to the fuel production. The reduction temperature is indicated by the color of the square.

In total, the CeP material produced 1.09 L of H₂ (4 cycles) and 2.32 L of CO (7 cycles). Figure 7 plots the oxygen production yields (squares) and the fuel productions (bars) depending on the reduction temperature. The cycles performed under low pressure during the reduction step are also indicated (hollow squares). A low pressure during the reduction step improved both the reduction extent (δ up to 0.056 in cycle #4) and the fuel production yield (315 $\mu\text{mol/g}$ in cycle #4), as previously reported [29,50]. In fact, decreasing the total pressure (by a factor of ~ 10) results in the same decrease of the oxygen partial pressure, which favors the reduction step. The same effect on p_{O_2} could be achieved by increasing the inert gas flow rate (for enhanced dilution), at the expense of a larger inert gas consumption (by a factor $\times 10$) to obtain the same effect as the total pressure reduction.

Under such appropriate operating conditions, a peak CO production rate approaching 10 mL/min/g was also achieved previously with microstructured ceria foams (exhibiting micron-sized grains forming an interconnected macroporous network within the struts) during their re-oxidation upon free cooling with a pure CO₂ stream after reduction at 1400°C [29,37]. This provides evidence that the ceria pellets with fibrous structure performed as well as ceria RPC structures designed as volumetric absorber. They could thus represent a promising alternative to less scalable RPCs manufactured by the replication method using polymer templates.

For the investigated cycling conditions, no significant performance decline was observed while increasing the number of cycles, and the material thermochemical stability was satisfactory (with good resistance to sintering) under the tested solar operating conditions. However, the long-term material stability would need being investigated over a higher number of cycles to confirm the absence of performance loss during extended periods and validate their applicability in a solar process. The main reason for performance decline in solar reactors is usually the presence of thermal gradients and

overheated zones that may cause material structure densification. Such issues may arise from low thermal conductivity and high optical thickness of the bed material. Thus, the heat transfer optimization and temperature homogenization in solar cavity receivers should always be targeted. A decrease of reactivity due to sintering and a loss of active surface area was previously observed with ceria felts [45] and 3DOM materials [19]. Generally, directly-irradiated solar reactors require using highly porous materials for volumetric radiation absorption, and the radiative opacity of particles bed or bulk fibers may be an obstacle for their application in direct heating mode. Hence, indirect heating may be more favorable. In the present study, the fibrous ceria pellets proved to be suitable for temperature-swing redox cycles in both direct and indirect heating modes, with high fuel production capacity, thermal stability and resistance to sintering. This compatibility with different reactor designs thus offers good material versatility for potential applications in solar fuel production.

4.3. Characterization of materials morphology, microstructure, and stability

The morphology and stability of the redox materials that were directly exposed to high-flux solar irradiation play a crucial role in their thermochemical performance. Given that these materials were cycled at high temperatures and subjected to steep temperature variations, it is necessary to analyze the samples microstructure before and after use in correlation with their relative performance and potential evolution.

The BET-specific surface area of CeP before cycling, measured by N₂ adsorption, was 0.50 m².g⁻¹ (vs. 0.31 and 0.25 m².g⁻¹, respectively for CTCe and CeF [41]). This could explain the higher fuel production rates obtained for CeP, compared to CTCe and CeF counterparts. The specific surface area of CeP measured after cycling was 0.38 m².g⁻¹ (thus denoting a moderate evolution after 11 cycles). This suggests that a temperature of 1400°C for the solar process was suitable to keep the high intrinsic reactivity of ceria fibers, whereas a low thermal stability was previously observed at higher temperatures [45,46].

The SEM images of the investigated materials after thermochemical cycles in the directly-heated solar reactor are shown in Figure 8. The microstructure of CeP consists of micron-sized ceria fibers with random orientations and interconnected open porosity. No noticeable change in morphology was observed for the cycled samples. The particles retained a porous and open microstructure after solar thermochemical cycles. No significant grain growth and no evidence of fiber degradation could be identified after cycling. The mean grain size was ~5-15 μm and the fiber length was ~30-50 μm. The fresh CeP material had grain sizes in the range 3-13 μm. SEM observations thus evidenced no significant variation of the material shape and morphology after cycling. The high fuel production rate of CeP can thus be attributed to the stable porous microstructure which favors solid-gas oxidation reactions.

Given that the pellets dimensions did not evolve significantly, changes in the density and porosity were not measurable. The bulk density of the CeP material was 1.8 g.cm^{-3} , which corresponds to an estimated porosity of $\sim 75.1\%$ when considering a value of 7.22 for the true density of ceria.

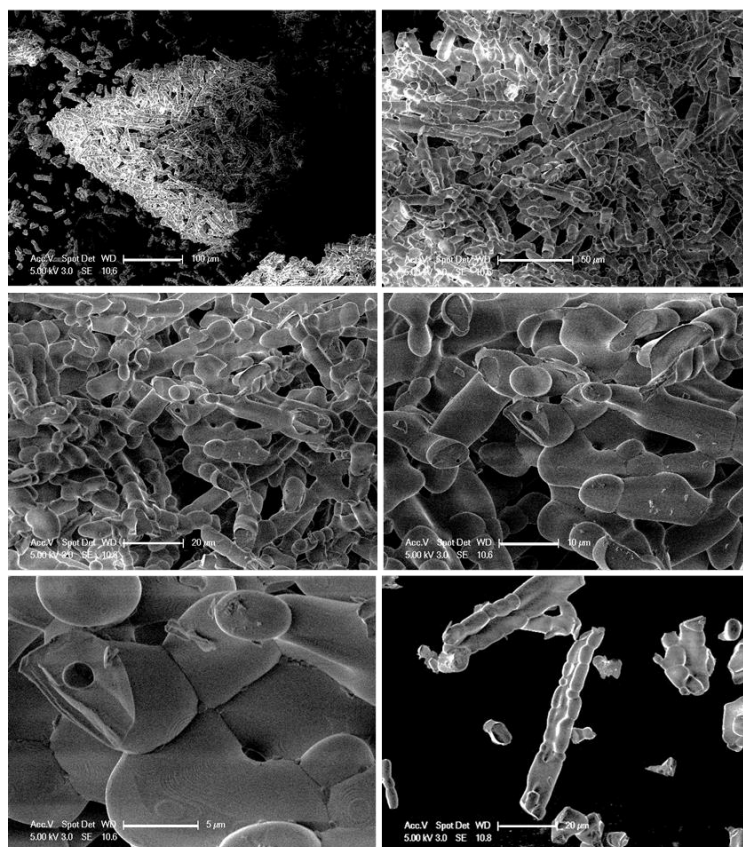


Figure 8: SEM micrographs showing the microstructure of cycliced fibrous ceria pellets (CeP) at different magnifications.

The ceria pellets morphology remained unchanged after being subjected to consecutive thermochemical cycles. In particular, no retraction was observed and the particle dimensions did not evolve. It can be underlined that a few particles of CeP reacted with the alumina tube in the upper part of the cavity (directly irradiated by concentrated sunlight), and led to the formation of CeAlO_3 . When the CeP reactive material was removed from the solar-heated cavity, a few particles at the top surface (that were in contact with the alumina center tube), showed a color change (from off-white to green, Figure 9a) and a local melting with alumina part of the cavity. XRD analysis confirmed the formation of CeAlO_3 by reaction between ceria and alumina (Figure 9b). Such reaction might be attributed to the high temperature underwent by the reacted particles (as they were located at the top of the cavity) in contact with alumina. However, due to the small amount of reactive material that had reacted with alumina, no performance decline attributed to this reaction could be observed. The mm-sized pellet particles were thus suitable for use in packed-bed solar reactors.

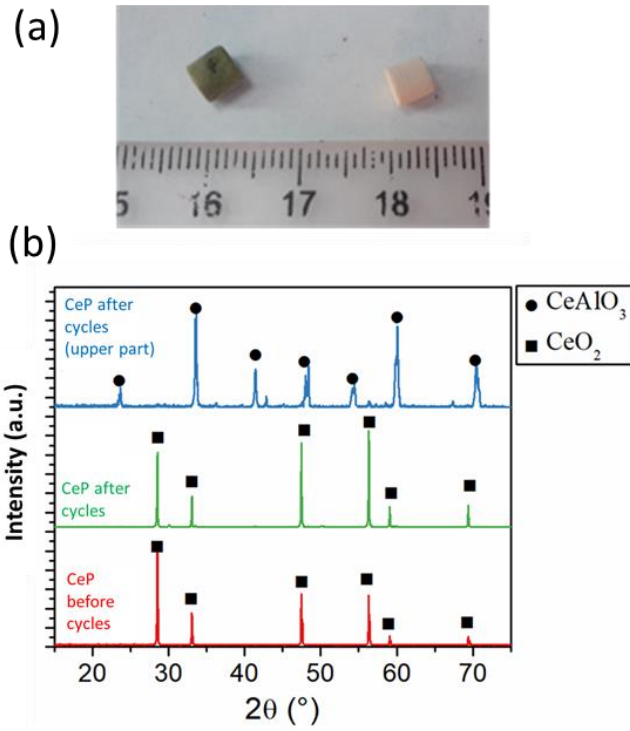


Figure 9: (a) Comparison of CeP materials after cycling (left: CeP which was in contact with alumina walls, and right: CeP which was not in contact with alumina), (b) XRD patterns of fresh CeP pellets before cycles, CeP pellets after cycles, and sintered CeP materials recovered from the upper part of the cavity (that reacted with alumina tube) after cycling in the directly-heated solar reactor.

Table 1. Operating parameters along with oxygen and fuel production yields during the investigated two-step thermochemical cycles in indirectly and directly-heated solar reactors (oxidation was performed off-sun during free cooling with oxidant gas injection (either H₂O or CO₂) starting at the mentioned temperature).

<i>Cycle #</i>	<i>T1 reduction step</i> (°C)	<i>Pressure</i> (bar)	<i>Ar flow rate during reduction</i> (L/min)	<i>O₂ produced</i> (μmol/g)	<i>T1 oxidation step</i> (°C)	<i>Oxidant gas (oxidant molar fraction)</i>	<i>Oxidant flow rate/Ar flow rate</i> (L/min)	<i>Fuel produced</i> (μmol/g)	<i>Peak fuel production rate</i> (mL/g/min)
<i>Indirectly-heated tubular solar reactor (m~10 g)</i>									
1	1400	0.878	0.25	64.5	<1010	H ₂ O (0.57)	0.33 / 0.25	126.2	1.17
2	1300	0.878	0.25	33.2	<930	H ₂ O (0.57)	0.33 / 0.25	59.8	0.49
3	1300	0.878	0.25	28.0	<930	H ₂ O (0.57)	0.33 / 0.25	61.2	0.51
4	1400	0.878	0.25	74.8	<1020	H ₂ O (0.57)	0.33 / 0.25	153.4	1.72
5	1400	0.878	0.25	69.8	<1030	H ₂ O (0.57)	0.33 / 0.25	145.5	1.63
6	1400	0.878	0.25	68.8	<940	H ₂ O (0.57)	0.33 / 0.25	143.3	2.30
7	1170	0.878	0.25	8.1	<1020	H ₂ O (0.57)	0.33 / 0.25	16.6	0.08
<i>Directly-heated solar reactor (m~63 g)</i>									
1	1391	0.878	1.20	89.0	<1059	CO ₂ (0.25)	0.40 / 1.20	172.7	1.34
2	1400	0.877	1.20	103.9	<1048	CO ₂ (1.00)	2.00 / 0.00	208.1	4.42
3	1401	0.873	1.20	112.0	<1050	CO ₂ (0.25)	0.40 / 1.20	194.7	1.53
4	1407	0.098	1.20	162.4	<1054	CO ₂ (1.00)	2.00 / 0.00	315.0	7.53
5	1403	0.872	1.20	117.0	<1055	H ₂ O (0.18)	0.27 / 1.20	200.9	1.03
6	1408	0.911	1.20	100.3	<1047	H ₂ O (0.40)	0.58 / 0.88	193.0	1.03
7	1405	0.912	1.20	102.5	<1052	H ₂ O (0.39)	0.45 / 0.70	193.1	0.81
8	1410	0.915	1.20	104.6	<955	H ₂ O (0.18)	0.27 / 1.20	188.0	1.26
9	1403	0.869	1.20	103.0	<954	CO ₂ (0.25)	0.40 / 1.20	151.5	2.44
10	1403	0.083	1.20	154.0	<1050	CO ₂ (1.00)	2.00 / 0.00	308.0	7.78
11	1403	0.083	1.20	148.0	<959	CO ₂ (1.00)	2.00 / 0.00	293.2	9.53

Table 2. Experimental conditions and fuel production performance for different ceria morphologies in two-step thermochemical redox cycles.

Ceria morphology	Heating mode	Cycling temperatures	Oxidizing gas	Peak fuel production rate (mL/min/g)	Fuel yield ($\mu\text{mol/g}$)	References
Felt	Solar simulator Direct heating	$T_{\text{red}}=1460\text{-}1647^\circ\text{C}$ $T_{\text{ox}}<927^\circ\text{C}$	$\text{CO}_2+\text{H}_2\text{O}$	1.9	262	Furler et al. [45]
Porous monolith	Solar simulator	$T_{\text{red}}=1620\text{-}1640^\circ\text{C}$	CO_2	4.6	192	Chueh et al. [33]
	Direct heating	$T_{\text{ox}}<900^\circ\text{C}$	H_2O	2.3	206	
RPC (foam)	Solar simulator	$T_{\text{red}}=1420^\circ\text{C}$	CO_2	0.127	65	Furler et al. [28]
	Direct heating	$T_{\text{ox}}<1000$				
RPC (foam)	Solar furnace Indirect heating	$T_{\text{red}}=1400^\circ\text{C}$ $T_{\text{ox}}=1050^\circ\text{C}\text{-}850^\circ\text{C}$	H_2O	0.6-0.8	115	Oliveira et al. [41]
Dual-scale porosity RPC (foam)	Solar simulator	$T_{\text{red}}=1450\text{-}1500^\circ\text{C}$	CO_2	1.2	276	Marxer et al. [47-48]
	Direct heating	$P_{\text{red}}=10\text{ mbar}$ $T_{\text{ox}}=700\text{-}1000^\circ\text{C}$				
Microstructured RPC (foam)	Solar furnace	$T_{\text{red}}=1400^\circ\text{C}$	CO_2	9.9	283	Haeussler et al. [29]
	Direct heating	$T_{\text{ox}}=986\text{-}825^\circ\text{C}$				
Cork-templated granules	Solar furnace	$T_{\text{red}}=1400^\circ\text{C}$	CO_2	1.9	151	Oliveira et al. [21, 41]
	Indirect heating	$T_{\text{ox}}=1050^\circ\text{C}\text{-}850^\circ\text{C}$	H_2O	1.0-1.4	162	
Ceria coating on inert foam	Solar furnace	$T_{\text{red}}=1400\text{-}1600^\circ\text{C}$	H_2O	-	116	Cho et al. [43]
	Direct heating	$T_{\text{ox}}=1100\text{-}900^\circ\text{C}$				
Commercial fibrous particles	Electric furnace	$T_{\text{red}}=1500^\circ\text{C}$ $T_{\text{ox}}=800^\circ\text{C}$	CO_2	8.4	51	Gladden and Davidson [46]
CeP fibrous pellets	Solar furnace Direct heating	$T_{\text{red}}=1400^\circ\text{C}$ $T_{\text{ox}}<959^\circ\text{C}$	CO_2	9.5	293	This work

5. Conclusion

This study focused on the investigation and optimization of solar fuels production by H_2O and CO_2 splitting reactions using non-stoichiometric ceria redox material as an oxygen carrier. A specific microstructure/morphology of the oxygen carrier was considered consisting of commercial-grade fibrous sintered pellets. The thermochemical performance of the ceria pellets was experimentally studied in packed-bed tubular and cavity-type solar reactors with either direct or indirect heating of the reacting materials. Different reactor designs were thus employed to study the effect of the operating parameters controlling the solar process performance during temperature-swing redox cycling. The fibrous ceria pellet morphology offered stable redox activity and microstructure, high fuel production performance, and was suitable for versatile solar redox applications.

The reduction is a thermally-activated process that proceeds with a continuous oxygen disincorporation from the oxide lattice as the temperature is increased. The reduction rate (O_2 evolution) thus immediately varied in response to the temperature change. High H_2 production rates (up to $2.3\text{ mL}\cdot\text{g}^{-1}\cdot\text{min}^{-1}$), comparing favorably to the performance of other ceria structures, were reached in the packed-bed tubular reactor with H_2/O_2 ratios approaching 2, providing compelling evidence of the complete fibrous material oxidation due to favorable morphology.

The material was further cycled in a directly-irradiated cavity-type reactor. The highest peak fuel production rate reached $\sim 9.5 \text{ mL}\cdot\text{g}^{-1}\cdot\text{min}^{-1}$ with a reduction step at $\sim 1400^\circ\text{C}$ under a reduced pressure of 83 mbar, and an oxidation step under 100% CO_2 starting at $\sim 950^\circ\text{C}$ upon cooling. The instant solar-to-fuel energy efficiency reached $\sim 9.4\%$. The low pressure during reduction also favored the fuel yield (beyond $300 \mu\text{mol/g}$), because the reduction extent was enhanced (δ up to 0.056). The decrease of the temperature during the oxidation step thermodynamically favored the fuel production rate. The increase of the CO_2 partial pressure also directly favored the kinetics (while decreasing the $p_{\text{CO}}/p_{\text{CO}_2}$ ratio, thus favoring thermodynamic equilibrium shift toward CO formation). The fibrous material outperformed most of the previously tested ceria morphologies including for instance templated RPC foams, felts, 3DOM or bio-inspired materials, applied to sustainable solar fuel production from water-splitting and CO_2 conversion. Such mm-sized pellet particles can potentially represent a promising alternative, comparing favorably to other less scalable structures, since they offered high fuel production capacity, thermal stability and resistance to sintering, with high potential for use in packed-bed reactors.

Acknowledgments:

The directly-irradiated solar reactor used in this work was funded by the French National Agency for Research (ANR, SUNFUEL project, contract N° ANR-16-CE06-0010). The authors thank Zircar Zirconia, Inc. (USA) for supplying the fibrous ceria materials, LNEG (Portugal) for SEM analysis, and R. Garcia for solar reactor design.

References:

- [1] C. Agrafiotis, M. Roeb, C. Sattler, A review on solar thermal syngas production via redox pair-based water/carbon dioxide splitting thermochemical cycles, *Renewable and Sustainable Energy Reviews*. 42 (2015) 254–285. <https://doi.org/10.1016/j.rser.2014.09.039>.
- [2] Y. Lu, L. Zhu, C. Agrafiotis, J. Vieten, M. Roeb, C. Sattler, Solar fuels production: Two-step thermochemical cycles with cerium-based oxides, *Progress in Energy and Combustion Science*. 75 (2019) 100785. <https://doi.org/10.1016/j.pecs.2019.100785>.
- [3] S. Abanades, Thermogravimetry Analysis of CO_2 and H_2O Reduction from Solar Nanosized Zn Powder for Thermochemical Fuel Production, *Ind. Eng. Chem. Res.* 51 (2012) 741–750. <https://doi.org/10.1021/ie202518k>.
- [4] M. Chambon, S. Abanades, G. Flamant, Solar thermal reduction of ZnO and SnO_2 Characterization of the recombination reaction with O_2 , *Chemical Engineering Science*. 65 (2010) 3671–3680. <https://doi.org/10.1016/j.ces.2010.03.005>.
- [5] S. Abanades, CO_2 and H_2O reduction by solar thermochemical looping using SnO_2/SnO redox reactions: Thermogravimetric analysis, *International Journal of Hydrogen Energy*. 37 (2012) 8223–8231. <https://doi.org/10.1016/j.ijhydene.2012.02.158>.

- [6] G. Levêque, S. Abanades, Kinetic analysis of high-temperature solid–gas reactions by an inverse method applied to ZnO and SnO₂ solar thermal dissociation, *Chemical Engineering Journal*. 217 (2013) 139–149. <https://doi.org/10.1016/j.cej.2012.11.105>.
- [7] G. Levêque, S. Abanades, J.-C. Jumas, J. Olivier-Fourcade, Characterization of Two-Step Tin-Based Redox System for Thermochemical Fuel Production from Solar-Driven CO₂ and H₂O Splitting Cycle, *Ind. Eng. Chem. Res.* 53 (2014) 5668–5677. <https://doi.org/10.1021/ie500206u>.
- [8] S. Abanades, I. Villafan-Vidales, CO₂ valorisation based on Fe₃O₄/FeO thermochemical redox reactions using concentrated solar energy, *Int. J. Energy Res.* 37 (2013) 598–608. <https://doi.org/10.1002/er.1953>.
- [9] P. Charvin, S. Abanades, F. Lemort, G. Flamant, Hydrogen Production by Three-Step Solar Thermochemical Cycles Using Hydroxides and Metal Oxide Systems, *Energy Fuels*. 21 (2007) 2919–2928. <https://doi.org/10.1021/ef0701485>.
- [10] P. Charvin, S. Abanades, E. Beche, F. Lemont, G. Flamant, Hydrogen production from mixed cerium oxides via three-step water-splitting cycles, *Solid State Ionics*. 180 (2009) 1003–1010. <https://doi.org/10.1016/j.ssi.2009.03.015>.
- [11] A. Haeussler, S. Abanades, J. Jouannaux, M. Drobek, A. Ayril, A. Julbe, Recent progress on ceria doping and shaping strategies for solar thermochemical water and CO₂ splitting cycles, *AIMS Materials Science*. 6 (2019) 657–684. <https://doi.org/10.3934/mat.2019.5.657>.
- [12] S. Ackermann, J.R. Scheffe, A. Steinfeld, Diffusion of Oxygen in Ceria at Elevated Temperatures and Its Application to H₂O/CO₂ Splitting Thermochemical Redox Cycles, *J. Phys. Chem. C*. 118 (2014) 5216–5225. <https://doi.org/10.1021/jp500755t>.
- [13] Abanades, Metal Oxides Applied to Thermochemical Water-Splitting for Hydrogen Production Using Concentrated Solar Energy, *ChemEngineering*. 3 (2019) 63. <https://doi.org/10.3390/chemengineering3030063>.
- [14] A. Haeussler, S. Abanades, J. Jouannaux, A. Julbe, Non-Stoichiometric Redox Active Perovskite Materials for Solar Thermochemical Fuel Production: A Review, *Catalysts*. 8 (2018) 611. <https://doi.org/10.3390/catal8120611>.
- [15] M.M. Nair, S. Abanades, Experimental screening of perovskite oxides as efficient redox materials for solar thermochemical CO₂ conversion, *Sustainable Energy Fuels*. 2 (2018) 843–854. <https://doi.org/10.1039/C7SE00516D>.
- [16] A. Riaz, P. Kreider, F. Kremer, H. Tabassum, J.S. Yeoh, W. Lipiński, A. Lowe, Electrospun Manganese-Based Perovskites as Efficient Oxygen Exchange Redox Materials for Improved Solar Thermochemical CO₂ Splitting, *ACS Appl. Energy Mater.* 2 (2019) 2494–2505. <https://doi.org/10.1021/acsaem.8b01994>.
- [17] S. Li, V.M. Wheeler, A. Kumar, M.B. Venkataraman, C.L. Muhich, Y. Hao, W. Lipiński, Thermodynamic Guiding Principles for Designing Nonstoichiometric Redox Materials for Solar Thermochemical Fuel Production: Ceria, Perovskites, and Beyond, *Energy Technol.* (2021) 2000925. <https://doi.org/10.1002/ente.202000925>.
- [18] N.D. Petkovich, S.G. Rudisill, L.J. Venstrom, D.B. Boman, J.H. Davidson, A. Stein, Control of Heterogeneity in Nanostructured Ce_{1-x}Zr_xO₂ Binary Oxides for Enhanced Thermal Stability and Water Splitting Activity, *J. Phys. Chem. C*. 115 (2011) 21022–21033. <https://doi.org/10.1021/jp2071315>.
- [19] S.G. Rudisill, L.J. Venstrom, N.D. Petkovich, T. Quan, N. Hein, D.B. Boman, J.H. Davidson, A. Stein, Enhanced Oxidation Kinetics in Thermochemical Cycling of CeO₂ through Templated Porosity, *J. Phys. Chem. C*. 117 (2013) 1692–1700. <https://doi.org/10.1021/jp309247c>.
- [20] C.D. Malonzo, R.M. De Smith, S.G. Rudisill, N.D. Petkovich, J.H. Davidson, A. Stein, Wood-Templated CeO₂ as Active Material for Thermochemical CO Production, *J. Phys. Chem. C*. 118 (2014) 26172–26181. <https://doi.org/10.1021/jp5083449>.

- [21] F.A.C. Oliveira, M.A. Barreiros, S. Abanades, A.P.F. Caetano, R.M. Novais, R.C. Pullar, Solar thermochemical CO₂ splitting using cork-templated ceria ecoceramics, *Journal of CO₂ Utilization*. 26 (2018) 552–563. <https://doi.org/10.1016/j.jcou.2018.06.015>.
- [22] W.C. Chueh, S.M. Haile, A thermochemical study of ceria: exploiting an old material for new modes of energy conversion and CO₂ mitigation, *Phil. Trans. R. Soc. A*. 368 (2010) 3269–3294. <https://doi.org/10.1098/rsta.2010.0114>.
- [23] Y. Hao, C.-K. Yang, S.M. Haile, High-temperature isothermal chemical cycling for solar-driven fuel production, *Phys. Chem. Chem. Phys.* 15 (2013) 17084. <https://doi.org/10.1039/c3cp53270d>.
- [24] N.R. Rhodes, M.M. Bobek, K.M. Allen, D.W. Hahn, Investigation of long term reactive stability of ceria for use in solar thermochemical cycles, *Energy*. 89 (2015) 924–931. <https://doi.org/10.1016/j.energy.2015.06.041>.
- [25] L.J. Venstrom, R.M. De Smith, Y. Hao, S.M. Haile, J.H. Davidson, Efficient Splitting of CO₂ in an Isothermal Redox Cycle Based on Ceria, *Energy Fuels*. 28 (2014) 2732–2742. <https://doi.org/10.1021/ef402492e>.
- [26] W.T. Gibbons, L.J. Venstrom, R.M. De Smith, J.H. Davidson, G.S. Jackson, Ceria-based electrospun fibers for renewable fuel production via two-step thermal redox cycles for carbon dioxide splitting, *Phys. Chem. Chem. Phys.* 16 (2014) 14271–14280. <https://doi.org/10.1039/C4CP01974A>.
- [27] A. Haeussler, S. Abanades, F.A. Costa Oliveira, M.A. Barreiros, A.P.F. Caetano, R.M. Novais, R.C. Pullar, Solar Redox Cycling of Ceria Structures Based on Fiber Boards, Foams, and Biomimetic Cork-Derived Ecoceramics for Two-Step Thermochemical H₂O and CO₂ Splitting, *Energy Fuels*. 34 (2020) 9037–9049. <https://doi.org/10.1021/acs.energyfuels.0c01240>.
- [28] P. Furler, J. Scheffe, M. Gorbar, L. Moes, U. Vogt, A. Steinfeld, Solar Thermochemical CO₂ Splitting Utilizing a Reticulated Porous Ceria Redox System, *Energy Fuels*. 26 (2012) 7051–7059. <https://doi.org/10.1021/ef3013757>.
- [29] A. Haeussler, S. Abanades, A. Julbe, J. Jouannaux, M. Drobek, A. Ayril, B. Cartoixa, Remarkable performance of microstructured ceria foams for thermochemical splitting of H₂O and CO₂ in a novel high-temperature solar reactor, *Chemical Engineering Research and Design*. 156 (2020) 311–323. <https://doi.org/10.1016/j.cherd.2020.02.008>.
- [30] M. Tou, R. Michalsky, A. Steinfeld, Solar-Driven Thermochemical Splitting of CO₂ and In Situ Separation of CO and O₂ across a Ceria Redox Membrane Reactor, *Joule*. 1 (2017) 146–154. <https://doi.org/10.1016/j.joule.2017.07.015>.
- [31] S. Abanades, A. Haeussler, A. Julbe, Thermochemical solar-driven reduction of CO₂ into separate streams of CO and O₂ via an isothermal oxygen-conducting ceria membrane reactor, *Chemical Engineering Journal*. 422 (2021) 130026. <https://doi.org/10.1016/j.cej.2021.130026>.
- [32] A. Haeussler, S. Abanades, J. Jouannaux, A. Julbe, Demonstration of a ceria membrane solar reactor promoted by dual perovskite coatings for continuous and isothermal redox splitting of CO₂ and H₂O, *Journal of Membrane Science*. 634 (2021) 119387. <https://doi.org/10.1016/j.memsci.2021.119387>.
- [33] W.C. Chueh, C. Falter, M. Abbott, D. Scipio, P. Furler, S.M. Haile, A. Steinfeld, High-Flux Solar-Driven Thermochemical Dissociation of CO₂ and H₂O Using Nonstoichiometric Ceria, *Science*. 330 (2010) 1797–1801. <https://doi.org/10.1126/science.1197834>.
- [34] R.C. Pullar, R.M. Novais, A.P.F. Caetano, M.A. Barreiros, S. Abanades, F.A.C. Oliveira, A Review of Solar Thermochemical CO₂ Splitting Using Ceria-Based Ceramics With Designed Morphologies and Microstructures, *Frontiers in Chemistry*. 7 (2019) 34. <https://doi.org/10.3389/fchem.2019.00601>.
- [35] G. Levêque, S. Abanades, Design and operation of a solar-driven thermogravimeter for high temperature kinetic analysis of solid–gas thermochemical reactions in controlled atmosphere, *Solar Energy*. 105 (2014) 225–235. <https://doi.org/10.1016/j.solener.2014.03.022>.

- [36] M.M. Nair, S. Abanades, Tailoring Hybrid Nonstoichiometric Ceria Redox Cycle for Combined Solar Methane Reforming and Thermochemical Conversion of H₂O/CO₂, *Energy Fuels*. 30 (2016) 6050–6058. <https://doi.org/10.1021/acs.energyfuels.6b01063>.
- [37] A. Haeussler, S. Abanades, A. Julbe, J. Jouannaux, B. Cartoixa, Solar thermochemical fuel production from H₂O and CO₂ splitting via two-step redox cycling of reticulated porous ceria structures integrated in a monolithic cavity-type reactor, *Energy*. 201 (2020) 117649. <https://doi.org/10.1016/j.energy.2020.117649>.
- [38] A. Haeussler, S. Abanades, A. Julbe, J. Jouannaux, B. Cartoixa, Two-step CO₂ and H₂O splitting using perovskite-coated ceria foam for enhanced green fuel production in a porous volumetric solar reactor, *Journal of CO₂ Utilization*. 41 (2020) 101257. <https://doi.org/10.1016/j.jcou.2020.101257>.
- [39] J. Randrianalisoa, S. Haussener, D. Baillis, W. Lipiński, Radiative characterization of random fibrous media with long cylindrical fibers: Comparison of single- and multi-RTE approaches, *Journal of Quantitative Spectroscopy and Radiative Transfer*. 202 (2017) 220–232. <https://doi.org/10.1016/j.jqsrt.2017.08.002>.
- [40] A. Singh, J. Lapp, J. Grobbel, S. Brendelberger, J.P. Reinhold, L. Olivera, I. Ermanoski, N.P. Siegel, A. McDaniel, M. Roeb, C. Sattler, Design of a pilot scale directly irradiated, high temperature, and low pressure moving particle cavity chamber for metal oxide reduction, *Solar Energy*. 157 (2017) 365–376. <https://doi.org/10.1016/j.solener.2017.08.040>.
- [41] F.A.C. Oliveira, M.A. Barreiros, A. Haeussler, A.P.F. Caetano, A.I. Mouquinho, P.M. Oliveira e Silva, R.M. Novais, R.C. Pullar, S. Abanades, High performance cork-templated ceria for solar thermochemical hydrogen production via two-step water-splitting cycles, *Sustainable Energy & Fuels*. 4 (2020) 3077–3089. <https://doi.org/DOI: 10.1039/d0se00318b>.
- [42] A. Le Gal, S. Abanades, G. Flamant, CO₂ and H₂O Splitting for Thermochemical Production of Solar Fuels Using Nonstoichiometric Ceria and Ceria/Zirconia Solid Solutions, *Energ. Fuel*. 25 (2011) 4836–4845. <https://doi.org/10.1021/ef200972r>.
- [43] H.S. Cho, N. Gokon, T. Kodama, Y.H. Kang, H.J. Lee, Improved operation of solar reactor for two-step water-splitting H₂ production by ceria-coated ceramic foam device, *International Journal of Hydrogen Energy*. 40 (2015) 114–124. <https://doi.org/10.1016/j.ijhydene.2014.10.084>.
- [44] P. Furler, J. Scheffe, D. Marxer, M. Gorbar, A. Bonk, U. Vogt, A. Steinfeld, Thermochemical CO₂ splitting *via* redox cycling of ceria reticulated foam structures with dual-scale porosities, *Phys. Chem. Chem. Phys.* 16 (2014) 10503–10511. <https://doi.org/10.1039/C4CP01172D>.
- [45] P. Furler, J.R. Scheffe, A. Steinfeld, Syngas production by simultaneous splitting of H₂O and CO₂ via ceria redox reactions in a high-temperature solar reactor, *Energy Environ. Sci.* 5 (2012) 6098–6103. <https://doi.org/10.1039/C1EE02620H>.
- [46] A.C. Gladen, J.H. Davidson, The morphological stability and fuel production of commercial fibrous ceria particles for solar thermochemical redox cycling, *Solar Energy*. 139 (2016) 524–532. <https://doi.org/10.1016/j.solener.2016.10.029>.
- [47] D. Marxer, P. Furler, M. Takacs, A. Steinfeld, Solar thermochemical splitting of CO₂ into separate streams of CO and O₂ with high selectivity, stability, conversion, and efficiency, *Energy Environ. Sci.* 10 (2017) 1142–1149. <https://doi.org/10.1039/C6EE03776C>.
- [48] D. Marxer, P. Furler, J. Scheffe, H. Geerlings, C. Falter, V. Batteiger, A. Sizmann, A. Steinfeld, Demonstration of the Entire Production Chain to Renewable Kerosene via Solar Thermochemical Splitting of H₂O and CO₂, *Energy Fuels*. 29 (2015) 3241–3250. <https://doi.org/10.1021/acs.energyfuels.5b00351>.
- [49] P. Furler, D. Marxer, M. Takacs, A. Steinfeld, Solar thermochemical reactor technology for splitting CO₂, *AIP Conference Proceedings*. 2033 (2018) 130005. <https://doi.org/10.1063/1.5067139>.

- [50] J.R. Scheffe, A. Steinfeld, Thermodynamic Analysis of Cerium-Based Oxides for Solar Thermochemical Fuel Production, *Energ. Fuel.* 26 (2012) 1928–1936. <https://doi.org/10.1021/ef201875v>.